NANO LETTERS

Letter

pubs.acs.org/NanoLett

Coherent, Mechanical Control of a Single Electronic Spin

Sungkun Hong,[†,∥] Michael S. Grinolds,[‡,∥] Patrick Maletinsky,[‡,∥] Ronald L. Walsworth,[‡,§] Mikhail D. Lukin,[‡] and Amir Yacoby*[,‡]

[†]School of Engineering and Applied Science, [‡]Department of Physics, and [§]Harvard-Smithsonian Center for Astrophysics, Harvard University, Cambridge, Massachusetts 02138, United States

Supporting Information

ABSTRACT: We demonstrate coherent quantum control of a single spin driven by the motion of a mechanical resonator. The motion of a mechanical resonator is magnetically coupled to the electronic spin of a single nitrogen-vacancy center in diamond. Synchronization of spin-addressing protocols to the motion of the driven oscillator is used to fully exploit the coherence of this hybrid mechanical-spin system. We demonstrate applications of this coherent mechanical spin-control technique to nanoscale scanning magnetometry.

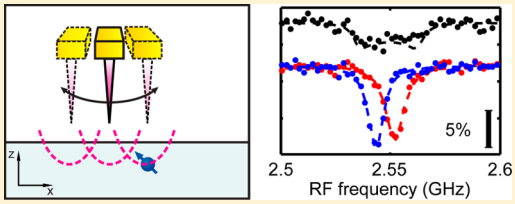

KEYWORDS: *Electron spin, mechanical resonator, hybrid mechanical-spin system, nitrogen-vacancy (NV) center, nanoscale magnetometry, nanoscale motion sensor*

The ability to control and manipulate spins via electrical,[1−3] magnetic,[4,5] and optical[6] means has generated numerous applications in metrology[7] and quantum information science[8] in recent years. A promising alternative method for spin manipulation is the use of mechanical motion, where the oscillation of a mechanical resonator can be magnetically coupled to a spin's magnetic dipole, which could enable scalable quantum information architectures[9] and sensitive nanoscale magnetometry.[10−12] To date, however, only population control of spins has been realized via classical motion of a mechanical resonator.[13−15] Here, we demonstrate coherent mechanical control of an individual spin under ambient conditions using the driven motion of a mechanical resonator that is magnetically coupled to the electronic spin of a single nitrogen-vacancy (NV) color center in diamond. Coherent control of this hybrid mechanical-spin system is achieved by synchronizing pulsed spin-addressing protocols (involving optical and radiofrequency fields) to the motion of the driven oscillator, which allows coherent mechanical manipulation of both the population and phase of the spin via motion-induced Zeeman shifts of the NV spin's energy, thus demonstrating full control of the spin's quantum state via mechanical means. We demonstrate applications of this coherent mechanical spin-control technique to sensitive nanoscale scanning magnetometry.

The magnetic coupling between spins and mechanical resonators has been recently investigated for imaging the locations of spins via magnetic resonance force microscopy[13,14] as well as for sensing nanomechanical resonator motion.[16] A scarcely explored resource in such coupled spin-resonator systems is the coherence of a driven resonator's motion, and here, we demonstrate that this motion can be used to fully control the quantum state of an individual electron spin. We employ an electronic spin associated with an NV center in diamond as the target spin due to the efficient optical initialization and readout of the NV spin,[17] as well as its long coherence time.[18] A single NV center is prepared near a bulk diamond surface (at a nominal depth of 10 nm, see Supporting Information), and its spin-state is read out optically through spin-dependent fluorescence.[17] The mechanical resonator is a quartz tuning fork with a microfabricated quartz tip attached at the end of one of its prongs. The tuning fork operates in a transverse oscillation mode with a resonant frequency of 41.53 kHz and oscillation amplitude that can be controllably varied up to 250 nm (see Figure 1 and Supporting Information). Magnetic coupling between the NV spin and the tuning fork resonator is provided by a 25 nm CoFe magnetic film evaporated onto the quartz tip (see Supporting Information). Consequently, the transverse mechanical motion of the tip generates an oscillatory magnetic field at the spin's location, which modulates the Zeeman splitting between the NV's energy levels (Figure 1b,c). We note that the tip is laterally positioned 500 nm from the NV spin, which keeps the NV outside from the range of the tip's motion. This helps to achieve linear coupling between the motion and the spin (see Supporting Information). To achieve coherent control of the target NV spin using the resonator's mechanical motion, we synchronize spin manipulation protocols to the driven oscillation of the mechanical resonator (Figure 1d). With this synchronization, the relative timing between applied radio-frequency (RF) pulses and the resonator motion is fixed, allowing for the resonator's motion to coherently and deterministically influence the NV spin state.

The pronounced coupling between the resonator's mechanical motion and the NV spin is measured with optically

Received: February 24, 2012
Revised: July 9, 2012
Published: July 16, 2012

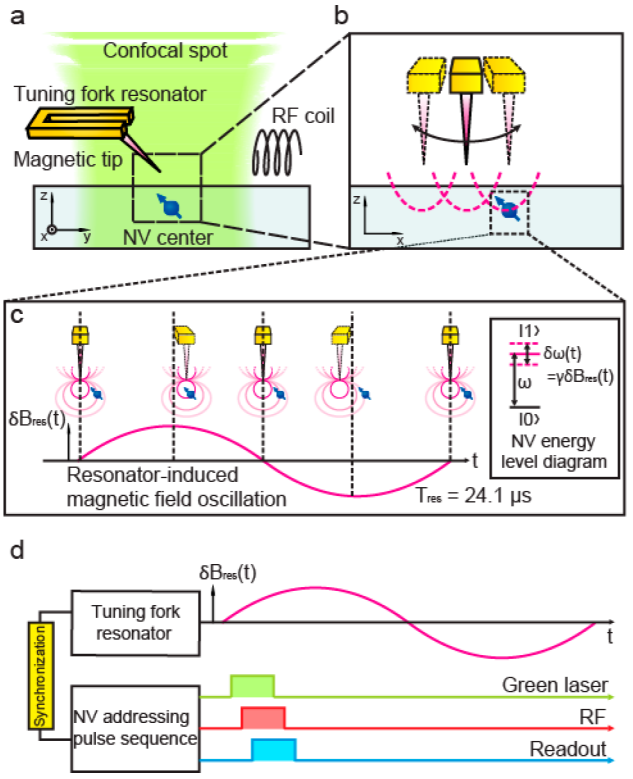

Figure 1. Coherent dynamics of a mechanical resonator and an electron spin. (a) Schematic of an electron spin of an NV center next to a tuning fork resonator. A magnetic tip provides coupling between the tuning fork resonator and the NV spin. Readout and addressing of the NV spin is provided through a confocal microscope and an RF coil. The details of the experimental setup are described in Grinolds et al.[22] (b,c) Coupling of the motion of the resonator to the electronic spin of the NV center. The local magnetic field at the position of the NV spin changes as a function of the resonator's motion due to the magnetic field gradient of the tip. This resonator-induced magnetic field oscillation, $\delta B_{res}(t)$, with the oscillation period, T_{res} = 24.1 μs, modulates the spin's dipole transition energy, $\delta\omega(t)$, through a Zeeman shift, $\delta\omega(t) = \gamma\delta B_{res}(t)$, where γ is the gyromagnetic ratio of the spin (inset). (d) Scheme for coherent coupling of the resonator's motion to the NV spin. The resonator's motion is synchronized to the NV addressing sequences. After this synchronization, the motion of the resonator influences the NV spin coherently with respect to the standard optical/RF pulse sequences that address the NV spin.

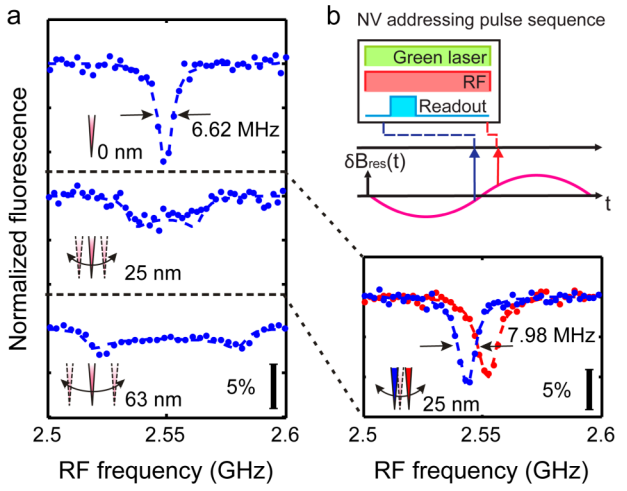

Figure 2. Spin-resonator coupling as observed by electron spin resonance (ESR). (a) Motion-induced broadening of ESR. As the amplitude of the resonator's oscillation is increased, the ESR line width broadens beyond its initial value (6.62 ± 0.49 MHz, here power-broadened by the applied RF field). The shape of ESR evolves to a bimodal form, owing to the simple harmonic oscillation of the resonator (see Supporting Information). (b) Stroboscopic ESR measurement. Measurements are taken synchronously to the motion of the resonator with 1 μs acquisition time. Having this short acquisition time compared to the oscillation period of the resonator (24.1 μs) results in stroboscopic ESR snapshots, which capture the applied tip field, and the corresponding shift in ESR, as a function of the resonator's position relative to the spin. The actual data (blue and red) are taken with the timings of −1.8 μs for the blue and 0.8 μs for the red relative to the node of the resonator's oscillation. The line width of the blue colored ESR is 7.98 ± 0.43 MHz, which is nearly recovered to the original line width of 6.62 MHz.

detected electron spin resonance (ESR). The ESR of the target NV center is acquired by sweeping the frequency of an applied RF field through the NV spin's magnetic dipole transition and collecting the resulting NV's spin-state-dependent fluorescence with lower (higher) fluorescence when RF field is on (off) resonance with the NV spin transition.[17] As the oscillation amplitude of the tuning fork increases, we observe a broadening in the ESR spectrum (Figure 2a), resulting from the larger magnetic field modulation associated with the greater range of motion of the resonator's magnetic tip. As the driving amplitude of the resonator is further increased, the ESR line shape becomes bimodal, which reveals the distribution of dwell-times of the magnetic tip as a function of its position during the oscillatory motion, with the two peaks representing the turning points of the oscillation trajectory (see Supporting Information). To deconvolve this time-averaged spectral broadening in the coupled dynamics of the NV spin and resonator, we perform stroboscopic ESR measurements synchronized to the resonator's motion (Figure 2b), which reveal the magnetic tip's position as a function of time via the tip-induced Zeeman shift of the NV's ESR resonance frequency. Figure 2b shows two example stroboscopic ESR spectra with shifted resonance frequencies consistent with the magnetic tip's position in its oscillatory cycle. Such measurements are acquired with an acquisition time (1 μs) much shorter than the resonator's oscillation period (24.1 μs), which enables stroboscopic readout of the NV spin's resonance frequency for a well-defined position of the magnetic tip. The observed remaining broadening of the ESR line width (full width at half-maximum) is within 20% of the value we find for an undriven magnetic tip (6.62 ± 0.49 MHz), which is due to the resonator's remnant motion during the nonzero acquisition time (see Supporting Information). The near-restoration of the zero-tip-motion ESR line width at arbitrary tip position confirms that the resonator motion is coherent with the spin addressing protocols.

This synchronization of the resonator's motion with respect to the external optical/RF control can be used for coherent control of both the population and phase of the target spin states. Population control (Figure 3) is achieved via an adiabatic fast passage.[19] The oscillation of the magnetic field induced by the magnetic tip motion modulates the NV ESR frequency. By fixing the applied RF frequency (ω_{RF}) to the center of this frequency modulation range, the target spin's population is adiabatically inverted each time the resonator-induced magnetic field brings the NV ESR frequency onto resonance with ω_{RF}. This spin population inversion occurs twice for each period of the resonator oscillation (here 24.1 μs), resulting in periodic

dx.doi.org/10.1021/nl300775c | Nano Lett. 2012, 12, 3920−3924

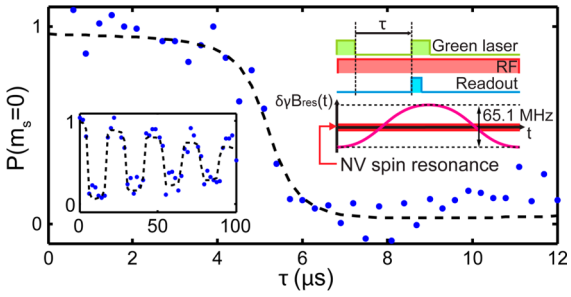

Figure 3. Population control of a spin with the mechanical motion of a resonator. The motion of the resonator periodically modulates the local magnetic field at the position of the target spin, and therefore modulates its spin resonance. Adiabatic spin inversions occur when the resonator sweeps the spin resonance through the frequency of an applied RF field (inset, right). The corresponding range of frequency sweep is 65.1 MHz, larger enough than the RF Rabi frequency, 6.25 MHz, to achieve high fidelity of spin inversion. Plotted is the population of the NV spin in the $m_s = 0$ state ($P(m_s = 0)$) as a function of delay between initialization and readout (τ). The left inset shows a periodic population modulation with multiple cycles and a period of 24.1 μs in accordance with the measured resonator frequency. Fits to the adiabatic passages take into account a finite RF Rabi frequency of 6.25 MHz (see Supporting Information). The decay in the inversion amplitude is determined by the spin-lifetime, T_1.

population inversion (i.e., spin flips). Note that such adiabatic population inversion can have a higher fidelity than conventional RF π-pulses, since it is robust against inhomogeneous variation in ESR frequency. It is especially useful for flipping ensembles of spins, where differing local environments for individual spins can otherwise limit control fidelity, provided that the tip-induced modulation of the field is larger than such inhomogeneous broadening.

Furthermore, synchronizing the resonator motion with an appropriate RF pulse sequence allows for high fidelity control of the target NV spin's phase. As a demonstration of such phase control, the NV spin is first prepared in a superposition state, using optical pumping followed by an RF $\pi/2$ pulse. Next, the time-varying magnetic field induced by the resonator's motion results in a detuning of the NV ESR frequency from ω_{RF}, causing the spin to acquire a differential phase relative to its precession at ω_{RF}. In order to accumulate the phase with high fidelity, and to minimize the effect of other incoherent magnetic field fluctuations, a Hahn echo sequence is employed and synchronized to the driven motion of the resonator (Figure 4a). By placing the pulse-sequence symmetrically with respect to the node of the resonator oscillation, the acquired phase is maximized for a given tip amplitude. For a fixed duration of the echo sequence (here, τ = 12 us), the amount of accumulated phase is proportional to the amplitude of the magnetic field oscillation, which is given by the oscillation amplitude of the magnetic tip displacement multiplied by the tip-induced magnetic field gradient along the direction of the tip motion. To read out the accumulated phase, a final RF pulse (here, $3\pi/2$) is applied to project the accumulated phase of the NV's spin onto a distribution of the state populations, which is then measured via spin-state-dependent fluorescence. Figure 4b shows an example of such resonator-induced spin phase accumulations, controlled by the amplitude of the resonator's oscillation.

In these demonstrations of coherent, mechanical control of a single NV spin, the rate of spin manipulation is set by the 41.53 kHz resonance frequency of the quartz tuning fork. However,

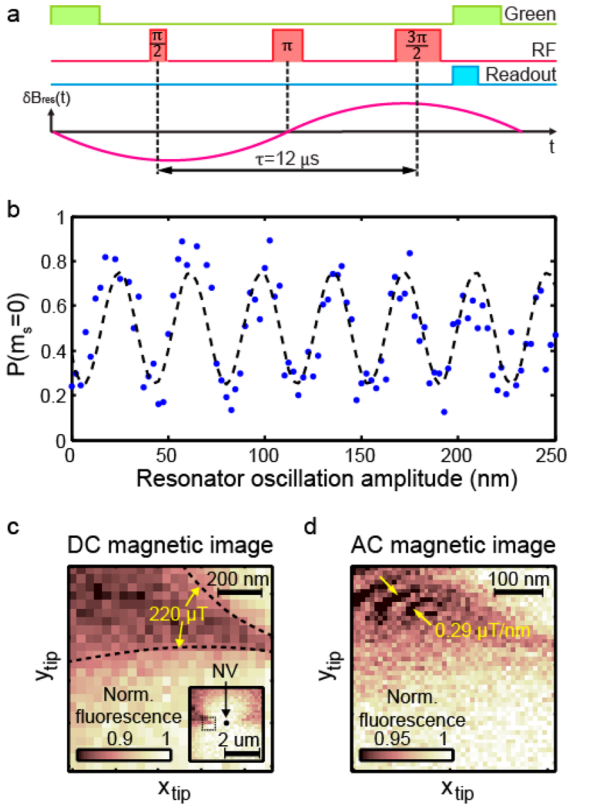

Figure 4. Phase control of a spin with the mechanical motion of a resonator and applications to magnetic imaging. (a) Phase accumulation scheme based on a Hahn echo sequence. The evolution time, τ, is fixed to 12 μs in this experiment. The echo sequence is symmetrically placed at the node of resonator's oscillatory motion, allowing for robust phase accumulation, which is only sensitive to the motion of the resonator, while canceling out slowly varying background magnetic fluctuations. (b) Phase accumulation of a spin as a function of the oscillation amplitude of the resonator. The accumulated phase is proportional to the magnetic field modulation induced by the resonator, which scales linearly with the oscillation amplitude of the resonator. When the phase is converted to the population of the NV spin in the $m_s = 0$ state ($P(m_s = 0)$) by a RF $3\pi/2$-pulse, we observe a sinusoidal oscillation of the population. (c) Scanning DC magnetometry with the NV spin. The external RF frequency is set on resonance with ESR in the absence of the magnetic tip. The change in local magnetic field at the position of NV results in ESR frequency shifts, which then changes the spin-state-dependent fluorescence. The larger scan image in the inset reveals a dipole-like pattern of the tip-induced magnetic field. The NV's position is marked as a black dot. The scan is zoomed to a region depicted by the dotted square box. The darker region is the region where the spin is near resonance with the external RF frequency. The field variation across the band is 220 μT. (d) Scanning AC magnetometry with the NV spin. The magnetic tip is scanned laterally with 20 nm oscillation amplitude. The modulation of the NV position relative to the magnetic target (here, the magnetic tip) produces a modulation of the magnetic signal from the source, providing a general method for adapting optimally sensitive AC magnetic imaging scheme. In comparison to DC magnetic image, we observe additional features, multiple fringes, which correspond to contours of constant magnetic field-gradient along the direction of the resonator's oscillation.

nanomechanical resonators can have resonance frequencies ranging up to nearly 1 GHz,[20,21] which would allow rapid control of target spins. For example, a resonator with 1 MHz frequency could perform more than 1000 coherent spin

dx.doi.org/10.1021/nl300775c | Nano Lett. 2012, 12, 3920−3924

manipulations within the demonstrated NV spin coherence time of a few milliseconds.[18]

With the demonstrated population and phase control, we have achieved coherent, mechanical control over the state of a single electron spin. This coherent mechanical spin-control technique enables new applications in sensitive, nanoscale metrology. In particular, electronic spins in NV centers have been recently identified as excellent magnetic field sensors because of their long coherence time and efficient optical readout,[10−12] even under ambient conditions. Previous work[11,12] showed that optimal magnetic field sensitivity is achieved when the target field is modulated with a period comparable to the NV's spin coherence time ("AC magnetometry"). However, such AC magnetometry cannot be applied a priori to targets with static magnetizations. Our coherent mechanical spin-control scheme provides a solution as the motion of the tip transforms a spatially varying, static magnetic field of a magnetic sample into a time-varying magnetic field at the position of the NV center. We demonstrate such mechanical-resonator-enabled AC magnetometry by performing scanning, nanoscale magnetic field imaging of our magnetized tip (Figure 4c,d). At first, we acquire a "DC magnetic image"[10,22] by scanning the magnetic tip laterally near a single NV center, where the external RF frequency is fixed on resonance with the NV ESR frequency in the absence of the tip, and the fluorescence change due to Zeeman shifts is monitored (Figure 4c). In this mode, the change in signal directly reflects the change in the local magnetic field at the position of NV. From the ESR spectrum (Figure 2a, top), the corresponding DC magnetic field sensitivity can be deduced to be 14 μT/(Hz)$^{1/2}$ (see Supporting Information). A resonance band with decreased fluorescence is formed where the tip's magnetic field along the NV axis is within one line width of the ESR. The width of this resonance band corresponds to the magnetic field variation along the NV axis of 220 μT. Next, we perform resonator-motion-enabled AC magnetometry (Figure 4d) where the same optical/RF-pulse sequence is used as for the phase-control experiment described above, while the driven motion of the magnetic tip is synchronized to the NV addressing protocols with fixed tip oscillation amplitude of 20 nm. We calculate our NV spin's AC magnetic field sensitivity to be 0.92 μT/(Hz)$^{1/2}$ (see Supporting Information), which constitutes a factor of 15 improvement over our DC experiment. In contrast to the DC magnetic image (Figure 4c), additional structures in the form of multiple parallel fringes in the resonance region are revealed. In this configuration, the NV center senses magnetic field variations along the direction of the tip oscillation, and the observed fringes (Figure 4d) correspond to contours of constant magnetic field gradients with neighboring fringes differing by a gradient of 0.29 μT/nm, or a field variation of 5.8 μT that is a factor of 40 smaller than that of DC image (see Supporting Information).

A particularly appealing application of our motion-enabled AC magnetometry could be sensitive nanoscale imaging of static, weak, and spatially varying magnetic features. Our magnetic imaging technique optimizes magnetic field sensitivity through AC magnetometry and should thereby be capable of detecting the magnetic moment of a single Bohr magneton within few seconds of data acquisition (see Supporting Information) at a 10 nm distance (which is the nominal depth of the prepared NV centers, see Supporting Information). It therefore offers the sensitivity required to detect local magnetic features down to a few Bohr magnetons in magnitude, provided that the NV spin can be brought within a few tens of nanometers of the sample. For example, this could be used to study much-debated graphene ferromagnetism,[23−27] where scanning nanoscale AC magnetometry can potentially provide local information of its magnetic origin. While in our demonstration of motion-enabled AC magnetometry, the NV spin-sensor is located in a fixed bulk diamond sample, our scheme can be readily applied to studying arbitrary samples in a scanning geometry. Such a scannable diamond device[28] has recently been developed, where an NV spin-sensor with 56 nT/(Hz)$^{1/2}$ sensitivity can be brought within a few tens of nanometers to the sample, making these applications of motion-locked AC magnetometry readily achievable.

An additional application of our coherent mechanical spin-control technique is motion sensing for nanoscale mechanical resonators. Such detection of motion, while routinely performed for microscale mechanical resonators using optical interferometry, remains challenging for nanoscale objects. Our mechanical spin-control scheme employs a single, atomically localized NV spin, thereby allowing nanoscale displacement and motion sensing. In principle, our demonstrated phase control scheme can be used to measure the amplitude and the phase of the motion of a resonator of interest. Using the measured magnetic tip field gradient of 18.4 μT/nm combined with the NV's AC field sensitivity, the oscillator amplitude sensitivity in our setup is estimated to be 49.8 pm/(Hz)$^{1/2}$, which is already comparable to the sensitivity (~10 pm/(Hz)$^{1/2}$) achieved by optical inteferometry of submicrometer sized resonators.[29] Similarly, the same scheme can be applied to measure the phase of the resonator's oscillatory motion with an estimated sensitivity of 5.1 mrad/(Hz)$^{1/2}$ at an oscillation amplitude of 10 nm.

The demonstrated sensitivity for metrology applications can be further optimized through a variety of experimentally demonstrated improvements. Such schemes of improvements include extending NV's spin coherence time[18,30] and enhancing photon collection efficiency.[28,31,32] Our displacement sensing scheme can also be improved by engineering higher magnetic field gradients. For example, by using state-of-the-art magnetic tips with a field gradient of 1 mT/nm,[14] an NV spin with T_2 of few milliseconds, and enhanced photon collection efficiencies, the displacement amplitude sensitivity of 22.8 fm/(Hz)$^{1/2}$ could potentially be achieved. Finally, we note that the techniques demonstrated here could be integrated with related methods for scanning-field-gradient spin MRI[22] and super-resolution optical imaging and coherent manipulation of proximal spins[33] with an ultimate goal of combined magnetic field sensitivity and spatial resolution to achieve real-time atomic-scale mapping of individual electron and nuclear spins in physical and biological systems of interest.

■ ASSOCIATED CONTENT

Supporting Information

Materials preparation, mathematical analysis of resonator-induced magnetic field fluctuation, simulation of spin's population control via resonator's motion, derivation of magnetic field sensitivity, simulation of imaging the magnetic field from the magnetized tip, simulation of imaging the magnetic field from a single electron spin. This material is available free of charge via the Internet at http://pubs.acs.org.

AUTHOR INFORMATION

Corresponding Author

*Address: LISE sixth floor, 11 Oxford Street, Cambridge, Massachusetts 02138. E-mail: yacoby@physics.harvard.edu. Phone: 617-495-1180. Fax: 617-495-4951.

Author Contributions

‖These authors contributed equally to this work.

Notes

The authors declare no competing financial interest.

ACKNOWLEDGMENTS

We gratefully acknowledge G. Balasubramanian and P. R. Hemmer for fruitful technical discussions as well as B. Hausmann and M. Loncar for instruction in the fabrication of NV center containing nanostructures. We acknowledge financial support from NIST and DARPA. S.H. acknowledges support from the Kwanjeong Scholarship Foundation for fellowship funding. M.S.G. is supported through fellowships from the Department of Defense (NDSEG program) and the NSF. P.M. acknowledges support from the Swiss National Science Foundation. This work was carried out in part at the Center for Nanoscale Systems (CNS), a member of the National Nanotechnology Infrastructure Network (NNIN), which is supported by the National Science Foundation under NSF award no. ECS-0336765. CNS is part of Harvard University.

REFERENCES

(1) Hanson, R.; Kouwenhoven, L. P.; Petta, J. R.; Tarucha, S.; Vandersypen, L. M. K. *Rev. Mod. Phys.* **2007**, *79* (4), 1217.

(2) Nowack, K. C.; Koppens, F. H. L.; Nazarov, Y. V.; Vendersypen, L. M. K. *Science* **2007**, *318*, 1430−1433.

(3) Foletti, S.; Bluhm, H.; Mahalu, D.; Umansky, V.; Yacoby, A. *Nat. Phys.* **2009**, *5* (12), 903−908.

(4) Poole, C. *Electron Spin Resonance*, 2nd ed.; Wiley: New York, 1983.

(5) Jelezko, F.; Gaebel, T.; Popa, I.; Gruber, A.; Wrachtrup, J. *Phys. Rev. Lett.* **2004**, *92*, 076401.

(6) Press, D.; Ladd, T. D.; Zhang, B.; Yamamoto, Y. *Nature* **2008**, *456* (7219), 218−221.

(7) Chernobrod, B. M.; Berman, G. P. *J. Appl. Phys.* **2005**, *97* (1), 014903−3.

(8) Nielsen, M. A.; Chuang, I. L. *Quantum Computation and Quantum Information*; Cambridge University Press: New York, 2000.

(9) Rabl, P.; Kolkowitz, S. J.; Koppens, F. H. L.; Harris, J. G. E.; Zoller, P.; Lukin, M. D. *Nat. Phys.* **2010**, *6* (8), 602−608.

(10) Balasubramanian, G.; Chan, I. Y.; Kolesov, R.; Al-Hmoud, M.; Tisler, J.; Shin, C.; Kim, C.; Wojcik, A.; Hemmer, P. R.; Krueger, A.; Hanke, T.; Leitenstorfer, A.; Bratschitsch, R.; Jelezko, F.; Wrachtrup, J. *Nature* **2008**, *455* (7213), 648−651.

(11) Maze, J. R.; Stanwix, P. L.; Hodges, J. S.; Hong, S.; Taylor, J. M.; Cappellaro, P.; Jiang, L.; Dutt, M. V. G.; Togan, E.; Zibrov, A. S.; Yacoby, A.; Walsworth, R. L.; Lukin, M. D. *Nature* **2008**, *455* (7213), 644−647.

(12) Taylor, J. M.; Cappellaro, P.; Childress, L.; Jiang, L.; Budker, D.; Hemmer, P. R.; Yacoby, A.; Walsworth, R.; Lukin, M. D. *Nat. Phys.* **2008**, *4* (10), 810−816.

(13) Rugar, D.; Budakian, R.; Mamin, H. J.; Chui, B. W. *Nature* **2004**, *430* (6997), 329−332.

(14) Mamin, H. J.; Poggio, M.; Degen, C. L.; Rugar, D. *Nat. Nanotechnol.* **2007**, *2* (5), 301−306.

(15) Wang, Y.-J.; Eardley, M.; Knappe, S.; Moreland, J.; Hollberg, L.; Kitching, J. *Phys. Rev. Lett.* **2006**, *97*, 227602.

(16) Arcizet, O.; Jacques, V.; Siria, A.; Poncharal, P.; Vincent, P.; Seidelin, S. *Nat. Phys.* **2011**, *7*, 879−883.

(17) Gruber, A.; Drabenstedt, A.; Tietz, C.; Fleury, L.; Wrachtrup, J.; Borczyskowski, C. v. *Science* **1997**, *276* (5321), 2012−2014.

(18) Balasubramanian, G.; Neumann, P.; Twitchen, D.; Markham, M.; Kolesov, R.; Mizuochi, N.; Isoya, J.; Achard, J.; Beck, J.; Tissler, J.; Jacques, V.; Hemmer, P. R.; Jelezko, F.; Wrachtrup, J. *Nat. Mater.* **2009**, *8* (5), 383−387.

(19) Slichter, C. P. *Principles of Magnetic Resonance*, 3rd ed.; Springer: Berlin, 1990; pp 20−24.

(20) Li, M.; Tang, H. X.; Roukes, M. L. *Nat. Nanotechnol.* **2007**, *2*, 114−120.

(21) Liu, N.; Giesen, F.; Belov, M.; Losby, J.; Moroz, J.; Fraser, A. E.; McKinnon, G.; Clement, T. J.; Sauerm, V.; Hiebert, W. K.; Freeman, M. R. *Nat. Nanotechnol.* **2008**, *3* (12), 715−719.

(22) Grinolds, M. S.; Maletinsky, P.; Hong, S.; Lukin, M. D.; Walsworth, R. L.; Yacoby, A. *Nat. Phys.* **2011**, *7*, 687−692.

(23) Yazyev, O. V.; Katsnelson, M. I. *Phys. Rev. Lett.* **2008**, *100* (4), 047209.

(24) Sepioni, M.; Nair, R. R.; Rablen, S.; Narayanan, J.; Tuna, F.; Winpenny, R.; Geim, A. K.; Grigorieva, I. V. *Phys. Rev. Lett.* **2010**, *105* (20), 207205.

(25) Oleg, V. Y. *Rep. Prog. Phys.* **2010**, *73* (5), 056501.

(26) Tada, K.; Haruyama, J.; Yang, H. X.; Chshiev, M.; Matsui, T.; Fukuyama, H. *Appl. Phys. Lett.* **2011**, *99* (18), 183111−3.

(27) Rao, S. S.; Jammalamadaka, S. N.; Stesmans, A.; Moshchalkov, V. V.; Tol, J. v.; Kosynkin, D. V.; Higginbotham-Duque, A.; Tour, J. M. *Nano Lett.* **2012**, *12* (3), 1210−1217.

(28) Maletinsky, P.; Hong, S.; Grinolds, M. S.; Hausmann, B. J. M.; Lukin, M. D.; Walsworth, R.; Loncar, M.; Yacoby, A. *Nat. Nanotechnol.* **2012**, *7* (5), 320−324.

(29) Kouh, T.; Karabacak, D.; Kim, D. H.; Ekinci, K. L. *Appl. Phys. Lett.* **2005**, *86* (1), 013106.

(30) de Lange, G.; Wang, Z. H.; Ristè, D.; Dobrovitski, V. V.; Hanson, R. *Science* **2010**, *330* (6000), 60−63.

(31) Babinec, T. M.; HausmannBirgit, J. M.; Khan, M.; Zhang, Y.; Maze, J. R.; Hemmer, P. R.; Loncar, M. *Nat. Nanotechnol.* **2010**, *5* (3), 195−199.

(32) Hadden, J. P.; Harrison, J. P.; Stanley-Clarke, A. C.; Marseglia, L.; Ho, Y.-L. D.; Patton, B. R.; O'Brien, J. L.; Rarity, J. G. *Appl. Phys. Lett.* **2010**, *97* (24), 241901.

(33) Maurer, P. C.; Maze, J. R.; Stanwix, P. L.; Jiang, L.; Gorshkov, A. V.; Zibrov, A. A.; Harke, B.; Hodges, J. S.; Zibrov, A. S.; Yacoby, A.; Twitchen, D.; Hell, S. W.; Walsworth, R. L.; Lukin, M. D. *Nat. Phys.* **2010**, *6* (11), 912−918.